PNAS RESEARCH ARTICLE | NEUROSCIENCE

Lateral entorhinal cortex afferents reconfigure the activity in piriform cortex circuits

Olivia Pedroncini[a,1], Noel Federman[a,2], and Antonia Marin-Burgin[a,2]

Affiliations are included on p. 8.

Edited by Kevin M. Franks, Duke University, Durham, NC; received July 19, 2024; accepted October 14, 2024 by Editorial Board Member J. Anthony Movshon

Odors are key signals for guiding spatial behaviors such as foraging and navigation in rodents. Recent findings reveal that odor representations in the piriform cortex (PCx) also encode spatial context information. However, the brain origins of this information and its integration into PCx microcircuitry remain unclear. This study investigates the lateral entorhinal cortex (LEC) as a potential source of spatial contextual information affecting the PCx microcircuit and its olfactory responses. Using mice brain slices, we performed patch-clamp recordings on superficial (SP) and deep (DP) pyramidal neurons, as well as parvalbumin (PV) and somatostatin (SOM) inhibitory interneurons. Concurrently, we optogenetically stimulated excitatory LEC projections to observe their impact on PCx activity. Results show that LEC inputs are heterogeneously distributed in the PCx microcircuit, evoking larger excitatory currents in SP and PV neurons due to higher monosynaptic connectivity. LEC inputs also differentially affect inhibitory circuits, activating PV while suppressing SOM interneurons. Studying the interaction between LEC inputs and sensory signals from the lateral olfactory tract (LOT) revealed that simultaneous LEC and LOT activation increases spiking in SP and DP neurons, with DP neurons showing a sharpened response due to LEC-induced inhibition that suppresses delayed LOT-evoked spikes. This suggests a regulatory mechanism where LEC inputs inhibit recurrent activity by activating PV interneurons. Our findings demonstrate that LEC afferents reconfigure PCx activity, aiding the understanding of how odor objects form within the PCx by integrating olfactory and nonolfactory information.

circuits | piriform cortex | lateral entorhinal cortex | inhibitory circuits | olfactory system

Significance

Primary sensory cortices are more complex than initially thought, encoding movement-related information and spatial maps. The olfactory piriform cortex (PCx) not only responds to odors but to other nonolfactory signals like the spatial context in which odors occur. This study investigates modulation of PCx by inputs from the lateral entorhinal cortex (LEC), candidate to carry contextual information. Using optogenetics, we found that LEC activation recruits excitatory and inhibitory circuits in PCx, that results in sharpening PCx principal neuron responses to odor inputs by reducing recurrent activity through PV interneurons. This reorganization suggests that LEC afferents could shift responses to favor the dominance of the odor pathway over the recurrent pathway, leading to a richer odor processing by integrating contextual information.

The complex and fluctuating nature of the environment in which we live requires the nervous system to be capable of generating flexible and adaptable internal representations of sensory stimuli. Previous works have demonstrated that this flexibility occurs early at the level of primary cortices, modulating the representation of a given stimulus depending on the task requirements (1). Recent studies on the olfactory processing of rodents have revealed the presence of spatial representations within the olfactory cortex when odors are associated with locations (2). Furthermore, it has been demonstrated that spatial and other nonolfactory information emerge in the olfactory cortex after learning (3). Finally, a very recent study involving single-neuron recordings in humans also revealed cross-modal integration in the olfactory cortex (4).

The piriform cortex (PCx) is the largest region of the olfactory cortex and plays a crucial role in encoding odor objects (5, 6). It is a trilaminar cortex and comprises two distinct populations of pyramidal neurons: the superficial pyramidal (SP) neurons located in layer 2 and deep pyramidal (DP) neurons in layer 3 (7). Both populations receive direct sensory afferents from the olfactory bulb (OB) through the lateral olfactory tract (LOT) (8). These dynamically interact with extensive recurrent or associational (ASSN) connections made by the PCx principal neurons (9–13). The proportion of inputs differs such that SP neurons are dominated by sensory afferents while DP neurons are mostly driven by recurrent circuits (14).

Moreover, afferent inputs not only excite PCx neurons but also recruit inhibitory circuits in a feedforward and feedback manner (9, 15–17). The feedback inhibition is primarily mediated by Parvalbumin (PV) and Somatostatin (SOM) interneurons (18). PV interneurons make perisomatic synapses with the principal neurons (15, 18) and are thought to regulate their spike activity (19). Conversely, SOM interneurons establish synapses on the proximal apical dendrites of the principal neurons influencing dendritic integration of afferent and recurrent inputs (20, 21). Therefore, it is the interplay between excitatory and inhibitory circuits in the PCx that determines the population of neurons activated in response to a stimulus (22).

Author contributions: O.P., N.F., and A.M.-B. designed research; O.P. performed research; O.P. and A.M.-B. analyzed data; and O.P., N.F., and A.M.-B. wrote the paper.

The authors declare no competing interest.

This article is a PNAS Direct Submission. K.M.F. is a guest editor invited by the Editorial Board.

[1]Present address: Sensory Circuits and Neurotechnology Laboratory, The Francis Crick Institute, London NW1 1AT, United Kingdom.

[2]To whom correspondence may be addressed. Email: nfederman@ibioba-mpsp-conicet.gov.ar or aburgin@ibioba-mpsp-conicet.gov.ar.

This article contains supporting information online at https://www.pnas.org/lookup/suppl/doi:10.1073/pnas.2414038121/-/DCSupplemental.

Published November 21, 2024.

In addition to the LOT and ASSN inputs, the PCx is reciprocally and extensively interconnected with higher-order cortical areas associated with emotional learning and mnemonic processes, such as the orbitofrontal cortex (23), the amygdala (24), and the perirhinal and entorhinal cortices (11, 25). All these regions send excitatory feedback projections to the PCx that may contribute to the formation of a broader and experience-dependent sensory representation in the PCx. One of these regions, the lateral entorhinal cortex (LEC), makes bidirectional connections with the PCx (26–29), as well as with the hippocampus. Its function has been associated with the encoding of memories of the spatial location of items and objects and the associations of items–outcome rules (30–34). The interaction of LEC afferents with the PCx circuit could confer nonolfactory information and spatial modulation to the odor representation, as has been observed in the activity of PCx neurons when animals learn to associate odors with spatial contexts and rewards (2, 3). However, the underlying mechanism remains unknown.

In this study, we aimed to understand how the projections of excitatory LEC neurons are integrated into the PCx microcircuit exploring the response of different subpopulations of PCx neurons to the activation of this input. We found that LEC afferents establish monosynaptic connections with SP neurons, and its activation leads to an enhancement of SP response to LOT stimulation. Notably, DP neurons exhibited a marked suppression of their late response to LOT stimulation which could be a consequence of the ASSN pathway silencing. Our findings suggest that the reduction in recurrence may be attributed to the activation of inhibitory circuits, with PV interneurons playing a central role. This could be a crucial mechanism for switching responses to favor the dominance of the LOT pathway over the recurrent pathway. Overall, these results highlight how nonolfactory aspects of animal experience, involving the LEC, can influence odor processing, potentially leading to a richer representation of odor objects.

Methods

Subject Details. To generate *Pvalb^{Cre}*;CAG^{FloxStopTom} (PV-Cre-floxTom) mice, *B6;129P2-Pvalbtm1(cre)Arbr/J (PV^{Cre})* mice) were crossed with *B6.Cg-Gt(ROSA)26Sortm14(CAG-tdTomato)Hze/J (Ai14)* conditional reporter mice. Cre heterozygous animals were used.

To generate *SOM^{Cre}*;CAG^{FloxStopTom} (SOM-Cre-floxTom) mice, *Ssttm2.1(cre)Zjh/J (SOM^{Cre})* were crossed with *B6.Cg-Gt(ROSA)26Sortm14(CAG-tdTomato)Hze/J (Ai14)* conditional reporter mice. Cre heterozygous animals were used.

Mice used in this study were both male and female and aged from 4 to 11 wk (see below for specific experiments). Mice were housed under controlled environment in a 12 h light/dark cycle, with food and water ad libitum.

Experimental protocol (2020-03-NE) was evaluated by the Institutional Animal Care and Use Committee of the IBioBA-CONICET according to the Principles for Biomedical Research involving animals of the Council for International Organizations for Medical Sciences and provisions stated in the Guide for the Care and Use of Laboratory Animals.

Animals and Surgery for Virus Delivery. For SP and DP recordings, we employed male C57BL/6J mice. For interneuron recordings, we use either sex PV-Cre-floxTom transgenic mice and either sex SOM-Cre-floxTom transgenic mice. All experimental mice were aged between 4 to 6 wk and weighed over 15 g at the time of surgical procedures.

For surgery, mice were anesthetized (150 μg ketamine/15 μg xylazine in 10 μL saline/g), and 400 to 450 nL of adenoviral vector pAAV-CaMKIIa-hChR2(H134R)-mCherry (AddGene) was infused at 125 nL/min into the left LEC using sterile microcapillary calibrated pipettes (Sigma) and stereotaxic references (coordinates from bregma: −3.6 mm anteroposterior, +3.9 mm mediolateral, −3 mm dorsoventral) to drive the expression of ChR2 in excitatory neurons of LEC (35, 36). The injection site was confirmed by cutting brain slices, fixing them, and obtaining confocal images of the fluorescence label of the injected area (Fig. 1).

Slice Preparation. After a 4 to 5-wk postviral injection period to allow Chr2 expression along infected neuronal projections, mice were anesthetized and killed by decapitation. Brains were removed into a chilled solution containing (mM) 110 choline-Cl^-, 2.5 KCl, 2.0 NaH_2PO_4, 25 $NaHCO_3$, 0.5 $CaCl_2$, 7 $MgCl_2$, 20 dextrose, 1.3 Na^+-ascorbate, and 3.1 Na^+-pyruvate. The left hemisphere was removed and slices (350 μm thick) were cut coronally in a vibratome and transferred to a chamber containing artificial cerebrospinal fluid (ACSF; mM): 125 NaCl, 2.5 KCl, 2.3 NaH_2PO_4, 25 $NaHCO_3$, 2 $CaCl_2$, 1.3 $MgCl_2$, 1.3 Na^+-ascorbate, 3.1 Na^+-pyruvate, and 10 dextrose (315 mOsm). Slices were bubbled with 95% O_2/5% CO_2 and maintained at 30 °C for approximately 1 h. before experiments started. Salts were acquired from Sigma-Aldrich (St. Louis, MO). When tetrodotoxin (TTX, 1 μM, Tocris) and 4-aminopyridine (4-AP, 100 μM, Sigma-Aldrich) were used, these were perfused into the bath solution.

Electrophysiological Recordings. Recordings were made from the posterior part of the anterior PCx covering a range from +0.1 to +1.5 mm anterior to Bregma. SP and DP recorded neurons were identified by their layer location (SP located in packed layer 2, DP in sparser layer 3) using infrared DIC video microscopy. PV and SOM interneurons expressing fluorescent protein dTomato were identified using a green LED source delivered through the epifluorescence pathway of the upright microscope.

Whole-cell recordings were performed using microelectrodes (4 to 10 MΩ) filled with (in mM) 130 CsOH, 130 D-gluconic acid, 2 $MgCl_2$, 0.2 EGTA, 5 NaCl, 10 HEPES, 4 ATP-tris, 0.3 GTP-tris, and 10 phosphocreatine. In experiments where spiking responses were evaluated, a potassium gluconate internal solution was used (in mM): 120 potassium gluconate, 4 $MgCl_2$, 10 HEPES buffer, 0.1 EGTA, 5 NaCl, 20 KCl, 4 ATP-tris, 0.3 GTP-tris, and 10 phosphocreatine (pH = 7.3; 290 mOsm).

Recordings were obtained using Multiclamp 700B amplifiers, (Molecular Devices), digitized, and acquired at 20 KHz onto a personal computer using the pClamp10 software. Membrane capacitance and input resistance were obtained from current traces evoked by a hyperpolarizing step of 10 mV. Series resistance was typically 10 to 20 MΩ. For the analysis of evoked currents, experiments were discarded if the series resistance was higher than 40 MΩ.

Evoked Postsynaptic Currents. Evoked monosynaptic excitatory postsynaptic currents (EPSC) and inhibitory postsynaptic currents (IPSC) were recorded after optogenetic stimulation executed by a 470 nm LED source delivered through the epifluorescence pathway of the upright microscope and commanded by the acquisition software. The stimulation protocol consisted of trains of 5 blue light pulses (10 Hz, pulse width = 0.5 ms, maximum intensity) delivered every 30 s.

EPSCs were isolated by voltage clamping SP, DP, PV, or SOM at the reversal potential of the IPSC measured for each individual neuron (∼−70 mV). In turn, IPSCs were recorded at the reversal potential of the EPSC (∼0 mV). When possible, both EPSC and IPSC were recorded from the same cell.

Charge was calculated as the integral of the current over a 90 ms window following the pulse. Excitatory current with peaks below −800 pA were considered spikes and were excluded from EPSC analysis. For latency analysis, recordings with average current peaks below 20 pA were excluded to ensure accurate onset determination. Latency was defined as the time between the peak of the pulse and the onset of the current. The onset was determined when the absolute value of the current exceeded a threshold of 2 times the SD of the baseline. Latencies of multiple pulses were included in Fig. 2*B*.

The excitatory to inhibitory balance was calculated as the proportion of excitatory charge over the total charge (sum of excitatory and inhibitory charge). This way of expressing the balance is more convenient than a simple ratio when there are values close to zero in the sample, as in our case.

Monosynaptic Responses. In order to dissect LEC monosynaptic inputs, a combination of Tetrodotoxin (1 μM) and 4-aminopyridine (100 μM) was added to the perfusion bath. TTX blocks voltage-gated sodium channels, preventing the generation of action potentials (APs), while 4-AP blocks potassium channels, depolarizing cell membranes and facilitating the release of neurotransmitter vesicles from stimulated terminals.

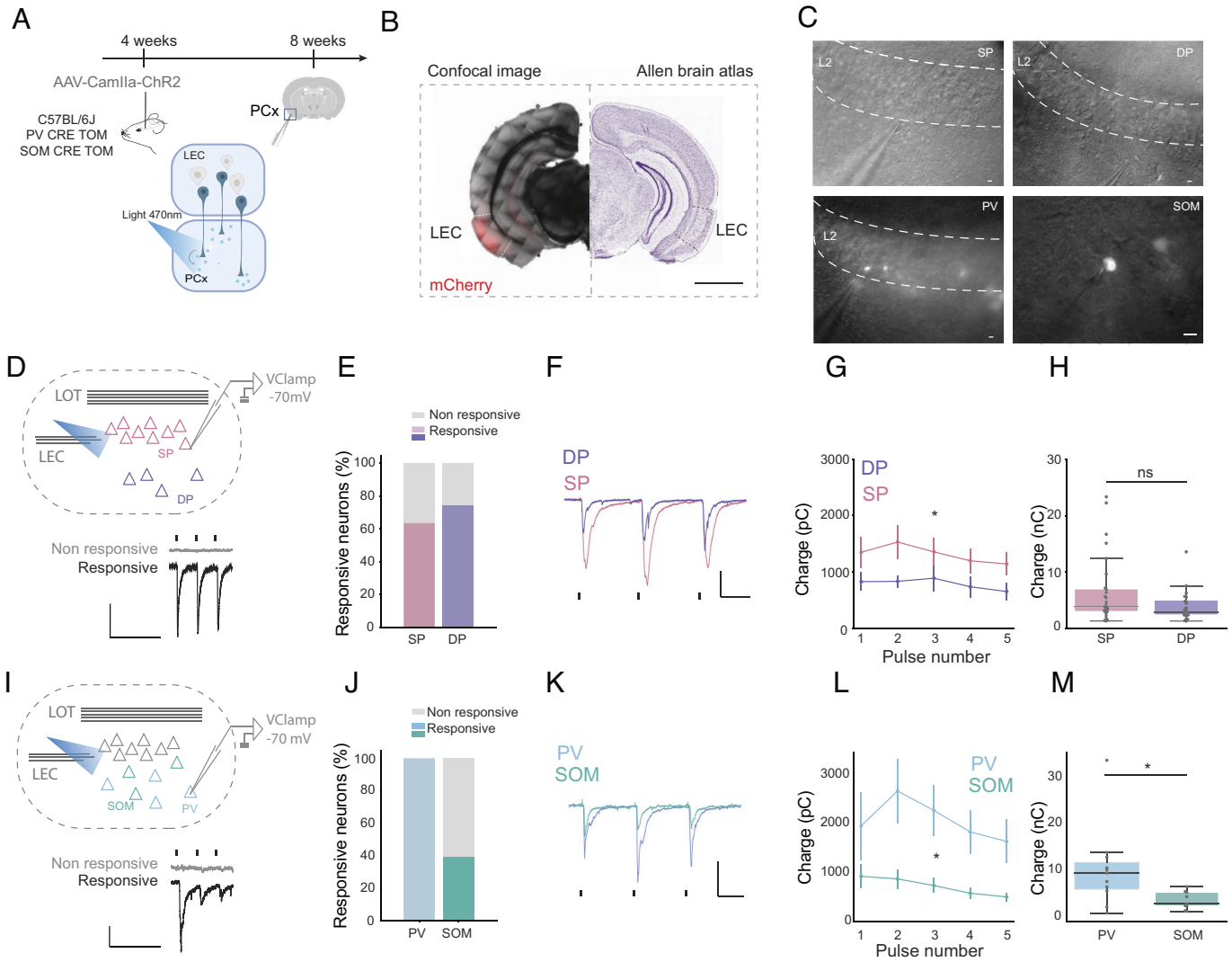

Fig. 1. Distinct effect of LEC input among PCx neuronal populations. (*A*) Experimental design. *Top*: Experimental timeline. 4-wk animals are injected with the adenovirus expressing ChR2; after 4 wk of viral expression, animals are killed, and acute brain slices of the piriform cortex are preserved for electrophysiological recordings. *Bottom*: Optogenetic strategy. Blue light over piriform cortex slice promotes neurotransmitter release from terminals of neurons expressing ChR2. (*B*) Confocal image of the injection site showing neurons expressing mCherry in LEC. (Scale bar, 2 mm.) (*C*) Representative images of electrophysiological recordings from Superficial Pyramidal neurons (SP), Deep Pyramidal neurons (DP), Parvalbumin Interneurons (PV), and Somatostatin interneurons (SOM). (Scale bar, 20 μm.) (*D–H*) Whole-cell recordings of EPSCs evoked by LEC stimulation in pyramidal neurons. (*D*) *Top*: Scheme illustrating experimental procedure. Individual SP and DP neurons are recorded in voltage-clamp holding the membrane at Vh = −70 mV while stimulating with blue light delivered at 10 Hz in a 5-pulses train. *Bottom*: Representative traces of a responsive neuron (black) and a nonresponsive neuron (gray). Black rectangles represent each stimulation pulse (only the first 3 pulses are shown). (Scale bar, x = 250 ms, y = 100 pA.) (*E*) Percentage of SP and DP responsive neurons (n_{SP} = 44 cells from 18 mice; n_{DP} = 31 cells from 17 mice). (*F*) Representative traces of a SP and a DP EPSC. (Scale bar, x = 50 ms, y = 100 pA.) (*G*) Charge of EPSC evoked by each pulse of LEC stimulation train in SP and DP responsive neurons (two-way ANOVA, SP versus DP: F = 4.591, *P* = 0.0376; variation in pulse number: F = 8.002, *P* = 0.0008, interaction: F = 0.0998, *P* = 0.9824; n_{SP} = 26 cells from 16 mice, n_{DP} = 21 cells from 15 mice). (*H*) Total charge of EPSCs evoked by the stimulation train (Mann–Whitney test, *P* = 0.0975, n_{SP} = 26 cells from 16 mice, n_{DP} = 21 cells from 15 mice). (*I–M*) Whole-cell recordings of EPSCs evoked by LEC stimulation in inhibitory interneurons. (*I*) *Top*: Scheme illustrating experimental procedure. Individual PV and SOM interneurons are recorded in voltage-clamp holding the membrane at Vh = −70 mV and stimulated with blue light with a 10 Hz 5-pulses train. *Bottom*: Representative traces of a responsive neuron (black) and a nonresponsive neuron (gray). Black rectangles represent each stimulation pulse (only the first 3 pulses are shown). (Scale bar, x = 250 ms, y = 20 pA.) (*J*) Percentage of PV and SOM responsive neurons (n_{PV} = 11 cells from 6 mice, n_{SOM} = 23 cells from 6 mice). (*K*) Representative traces of a PV and a SOM EPSC. (Scale bar, x = 50 ms, y = 100 pA.) (*L*) Charge of EPSC evoked by each pulse of LEC stimulation train in PV and SOM responsive neurons (two-way ANOVA, PV versus SOM: F = 5.8, *P* = 0.0367; variation in pulse number: F = 5.095, *P* = 0.0084; interaction: F = 1.918, *P* = 0.1166; nPV = 11 cells from 6 mice, nSOM = 9 cells from 6 mice). (*M*) Total charge of EPSCs evoked by the stimulation train (Mann–Whitney test: *P* = 0.0159, nPV = 11 cells from 6 mice, nSOM = 9 cells from 6 mice).

At least 5 min were allowed to pass between the addition of the drugs and the assessment of their effect. A threshold of −15 pA was established to determine whether a neuron responded or not under the influence of the TTX and 4-AP drugs.

Spiking Response. Single APs were identified when the membrane voltage exceeded a threshold set at V = 50 mV. To study LOT responses, a stimulation protocol comprising 5-pulse trains (10 Hz, pulse width = 0.2 ms, threshold intensity) delivered by an electrode in the LOT was applied every 30 s. To study responses to both LOT and LEC pathways, this protocol was combined with optogenetic stimulation (5-pulse trains at 10 Hz, pulse width = 0.5 ms, maximum intensity) aligning the onset of electrical and light pulses.

A search window of 70 ms was established following each stimulation pulse for AP detection. Latency was calculated as the time between the peak of the pulse and the peak of the action potential. APs with latencies smaller than 2 ms were excluded from the analysis, as they were considered to result from direct rather than synaptic stimulation.

Quantification and Statistical Analysis. Unless otherwise specified, data are presented as mean ± SEM. Normality was assessed using Shapiro–Wilk's test,

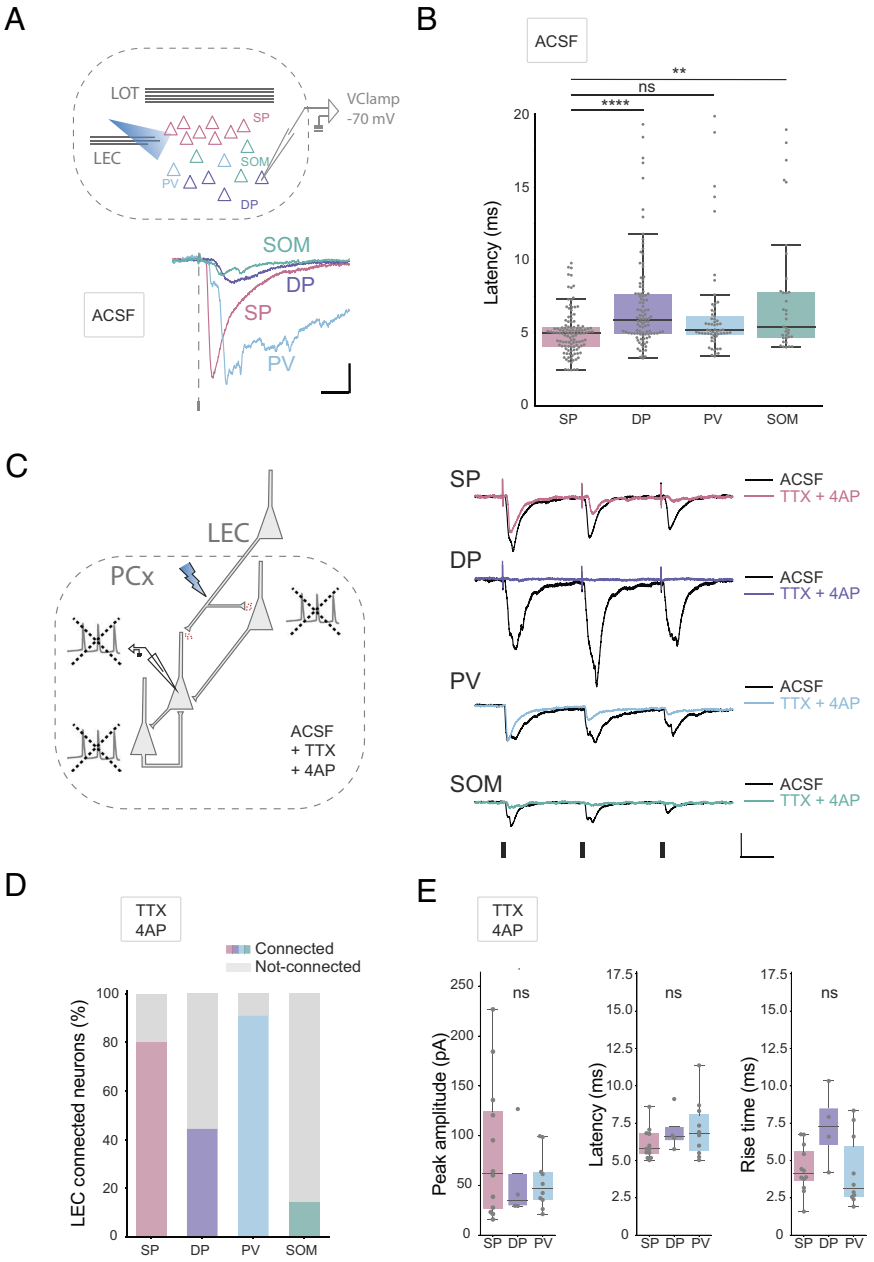

Fig. 2. Excitatory LEC projection contacts preferentially SP and PV neurons in the PCx. (*A*) *Top*: Scheme illustrating experimental procedure. Individual SP, DP, PV, and SOM neurons are recorded in voltage-clamp holding the membrane at Vh = −70 mV while stimulating with blue light delivered at 10 Hz in a 5-pulses train. *Bottom*: Representative traces showing a difference in latencies of the EPSC (only first pulse is shown). (Scale bar, x = 10 ms, y = 50 pA.) (*B*) Latencies to the onset of EPSC for different neuronal populations. Each point corresponds to an EPSC evoked by a single pulse of the train (all pulses are included). Boxes indicate median and quartiles (Kruskal–Wallis test, statistic = 28.82, $P < 0.0001$; Dunn's multiple comparison, SP versus DP: mean rank diff = −62.55, $P < 0.0001$; SP versus PV: mean rank diff = −35.96, $P = 0.075$; SP versus SOM: mean rank diff = −57.77, $P = 0.006$; nSP = 119 events from 24 cells from 12 mice, nDP = 102 events from 24 cells from 15 mice, nPV = 60 events from 12 cells from 6 mice, nSOM = 35 events from 7 cells from 5 mice). (*C*) *Left*: Pharmacological strategy to dissect monosynaptic connections. The combination of Tetrodotoxin (TTX) and 4-aminopyridine (4-AP) in the bath prevents neurons from firing action potentials, effectively maintaining membrane depolarization and thereby facilitating neurotransmitter release from stimulated terminals. *Right*: Representative traces of EPSCs from SP, DP, PV, and SOM neurons before (CTR in Black) and after (in colors, TTX+4AP) the infusion of the drugs into the bath. (Scale bar, x = 50 ms, y = 50 pA.) (*D*) Percentage of connected neurons (SP = 80%, DP = 44.44%, PV = 90.9%, SOM = 14.3%; nSP = 15 cells from 6 mice, nDP = 9 cells from 3 mice, nPV = 11 cells from 3 mice, nSOM = 7 cells from 3 mice). (*E*) Peak amplitude, latency, and rise time of light evoked monosynaptic currents recorded in TTX and 4AP (Kruskal–Wallis test, Peak Amplitude: statistic = 1.15, $P = 0.57$; Latency: statistic = 4.62, $P = 0.1$; Rise Time: statistic = 2.98, $P = 0.23$; %; nSP = 12 cells from 4 mice, nDP = 4 cells from 3 mice, nPV = 10 cells from 3 mice).

D'Agostino & Pearson omnibus test, or Kolmogorov–Smirnov's test, with a *P* value of 0.05. Two-tailed ordinary, one-sample or paired *t* test was used for single comparisons, and ordinary or repeated-measures ANOVA for multiple comparisons, with post hoc Tukey's test. For non-normal distributions, comparisons were made using nonparametric tests such as the Mann–Whitney test and Wilcoxon signed-rank test. Statistical details of experiments can be found in the figure legends and *Results*.

Results

LEC Afferents Are Heterogeneously Distributed in the PCx Microcircuit. In order to explore the effect of LEC activation in the piriform microcircuit, we injected an adeno-associated virus carrying the photoactivatable protein channelrhodopsin-2 (ChR2) under a promoter of excitatory neurons (Camk2a) in LEC. We then obtained ipsilateral PCx brain slices and stimulated them with blue light (Fig. 1 *A* and *B*), while performing electrophysiological whole-cell recordings from different groups of excitatory and inhibitory neurons in PCx (Fig. 1*C*). We first recorded, in voltage-clamp mode, excitatory postsynaptic currents (EPSC) from two populations of pyramidal cells, SP and DP neurons, in response to LEC stimulation with a train of 5 pulses at a frequency of 10 Hz (Fig. 1*D*). This frequency falls within the range of theta oscillations (7 to 12 Hz) which corresponds to the activity evoked by odors in OB and LEC (37). We observed LEC-evoked EPSCs in 62.8% of the recorded SP neurons and in 74.2% of the DP neurons (Fig. 1*E*). Comparing those responsive neurons, we found that SP neurons receive significantly larger currents than DP neurons along the stimulation train (Fig. 1 *F* and *G*). However, when we compared the total charge evoked by the sum of the five pulses of the train, we observed a nonsignificant trend that, we believe, is due to a big variability within each group (Fig. 1*H*).

Next, we studied the interaction of LEC inputs with inhibitory circuits of PCx. We recorded LEC-evoked EPSCs from two of the main populations of GABAergic neurons present in PCx, PV, and SOM interneurons. For these experiments, we used transgenic mouse lines PV-Cre-floxTom and SOM-Cre-floxTom that allowed us to identify PV-IN and SOM-IN respectively (Fig. 1*C*). We detected excitatory responses in 100% of PV and only 39.1% of SOM interneurons (Fig. 1 *I* and *J*). Taking the subset of responsive

neurons, we analyzed EPSCs evoked by a 5 pulses train stimulation of blue light and observed that the currents in PV interneurons were larger than those in SOM (Fig. 1 *K* and *L*). We obtained the same result comparing the total charge of the stimulation train (Fig. 1*M*).

LEC Projections Preferentially Contact SP Neurons and PV Interneurons. As PCx neurons are extensively interconnected forming a recurrent network, we were uncertain whether the EPSCs that we recorded were due to direct monosynaptic input from LEC or, alternatively, recurrent excitation. To address this, we first quantified the latency of EPSCs for each neuronal population (Fig. 2 *A* and *B*). Both SP and PV neurons showed similar onset latencies. SP latencies were significantly shorter than the ones of DP and SOM neurons (Fig. 2*B*). The difference in the latency to evoke a postsynaptic current could be due to the fact that some of the neurons receive monosynaptic connections while others might be responding to the recurrent activation that originated in the monosynaptically connected cells.

In order to further clarify the connectivity of LEC projections, we recorded evoked EPSCs in the presence of Tetrodotoxin (TTX) and 4-aminopyridine (4-AP). This combination of drugs allows dissecting monosynaptic inputs by suppressing action potential (AP) firing while promoting neurotransmitter release from depolarized terminals (Fig. 2*C*). We recorded LEC evoked EPSCs from SP, DP, PV, and SOM neurons after the infusion of TTX and 4-AP. Neurons were classified as "connected" or "not-connected" by establishing a minimal response threshold (EPSCamplitude = −15 pA). As expected, a high percentage of SP and PV neuronal populations were connected (80% and 90.9% respectively); whereas only 44.4% of DP neurons and 14.3% of SOM interneurons showed monosynaptic LEC connections (Fig. 2*D*). We found that neurons that received LEC monosynaptic connections showed indistinguishable excitatory currents evoked by the first light pulse (SOM interneurons were not included due to the low number of connected neurons) (Fig. 2*E*). Altogether, these results suggest that the majority of LEC responses in DP and SOM neurons measured in ACSF, where mono- and polysynaptic transmission occur, are mediated by polysynaptic pathways. This is likely due to recurrent activity triggered by the spiking of excitatory neurons monosynaptically connected to LEC. The heterogeneous connectivity of LEC afferents in PCx, particularly the strong connectivity with PV interneurons, suggests an important role in the modulation of PCx activity.

Activation of LEC Afferents Induces a Functional Reorganization of PCx Inhibition. Since PV inhibitory interneurons receive direct excitatory synapses from LEC, we asked whether LEC activation induces inhibitory postsynaptic currents (IPSCs) across distinct neuronal populations within the circuit (Fig. 3 *A* and *I*). We observed LEC-evoked IPSCs in 25% of the recorded SP neurons and in 50% of the DP neurons (Fig. 3*B*). We did not find any significant difference between them when we compared the inhibitory charge per pulse (Fig. 3 *C* and *D*) or the total charge (Fig. 3*E*).

To understand how individual neurons integrate the inputs resulting from LEC activation, we evaluated the excitation to inhibition balance (E/I balance) calculated as the amount of excitation over the sum of excitation and inhibition (E/E + I). We considered all the neurons that we recorded at both V_h = −70 mV and V_h = 0 mV (Fig. 3*F*). Neurons that exhibited neither EPSCs nor IPSCs in response to LEC activation were excluded from the analysis. The two groups of pyramidal neurons showed a difference in the E/I balance along the train (Fig. 3*G*). For SP neurons, the E/I balance was close to 0.5 indicating that a given magnitude of excitatory current elicits a correspondingly similar inhibitory current. In contrast, for DP neurons, inhibitory charge overcame excitatory charge leading to a "negative" E/I balance (Fig. 3*H*). This suggests that activation of LEC inputs would result in an overall activation of SP and an inhibition of DP neurons.

In addition, we recorded IPSCs and calculated E/I balance for PV and SOM interneurons (Fig. 3 *I*–*K*). We did not find any difference in the inhibitory charge per pulse (Fig. 3*L*) or the total charge (Fig. 3*M*). Consistent with the difference in EPSCs previously reported, SOM interneurons show responses dominated by inhibition whereas PV interneurons tend to be dominated by excitation (Fig. 3*N*). The E/I balance per pulse differed between PV and SOM interneurons (Fig. 3*O*). SOM interneurons showed a striking negative (under 0.5) mean E/I balance meaning that inhibitory inputs predominate over excitatory ones (Fig. 3*P*). In the case of PV interneurons, even though we did not observe a significant E/I balance above 0.5 (Fig. 3*P*), we detected spiking activity in response to light (unlike the rest of the neuronal populations recorded) (*SI Appendix*, Fig. S1). Because SOM interneurons are known to inhibit PV cells (20), their net inhibition by LEC activation could further enhance activation of PV. These results demonstrate that inputs arriving from LEC have a different impact in both populations of interneurons, which would lead to a reorganization of the PCx output.

LEC Afferent Activation Modulates Pyramidal Spiking Responses to LOT Inputs. The effect of stimulating the isolated LEC pathway resulted in a differential activation of different populations of neurons in PCx. We then wanted to evaluate whether this input could modulate how pyramidal neurons respond to afferent input arriving from the olfactory bulb. To study this, we recorded the spiking activity of SP and DP neurons in response to either LOT electrical stimulation, or combined LOT and LEC simultaneous stimulation (light stimulation of LEC alone did not induce spikes in these neurons). We set the intensity of the stimulation electrode placed in the LOT at the threshold level and stimulated with a train of 5 pulses delivered at 10 Hz. For combined stimulation of LOT and LEC, we superimposed a 5 pulses train at 10 Hz of blue light at a fixed intensity, to the LOT stimulation protocol (Fig. 4*A*).

We observed an increase in the number of evoked spikes when stimulating the combined pathways for both SP and DP neurons (Fig. 4*B*). However, when we analyzed the temporal profile of these responses (i.e., the latency to the peak of each action potential) we noticed, only for DP neurons, a temporal shift toward earlier responses when both pathways were stimulated (Fig. 4 *C* and *D*). It is worth noting that the basal response of SP neurons to LOT stimulation exhibits an earlier and sharper distribution compared to the spiking response of DP neurons. This can be explained due to the prevailing influence of LOT input over associational one on SP neurons. The broad basal distribution of DP neurons is consistent with a larger influence of the ASSN pathway, which tend to produce a second peak at around 20 ms, as has been previously shown (13). From this result, we propose that LEC predominantly affects the recurrence of the circuit, thereby producing a more pronounced effect on DP neurons.

To better evaluate the timing within which LEC inhibits the occurrence of late spikes, we stimulated LOT with a sequence of 2 pulses varying the intertrial interval (ITI) from 15 to 30 ms (*SI Appendix*, Fig. S2*A*). The stimulation intensity was maintained such that the second pulse reached the threshold level. We quantified the percentage of spike occurrences following the second pulse and compared this with a condition in which we superimposed LEC stimulation with a single light pulse in coincidence with the first LOT pulse. We found that when adding LEC stimulation, the percentage of spike occurrence elicited by the second LOT pulse

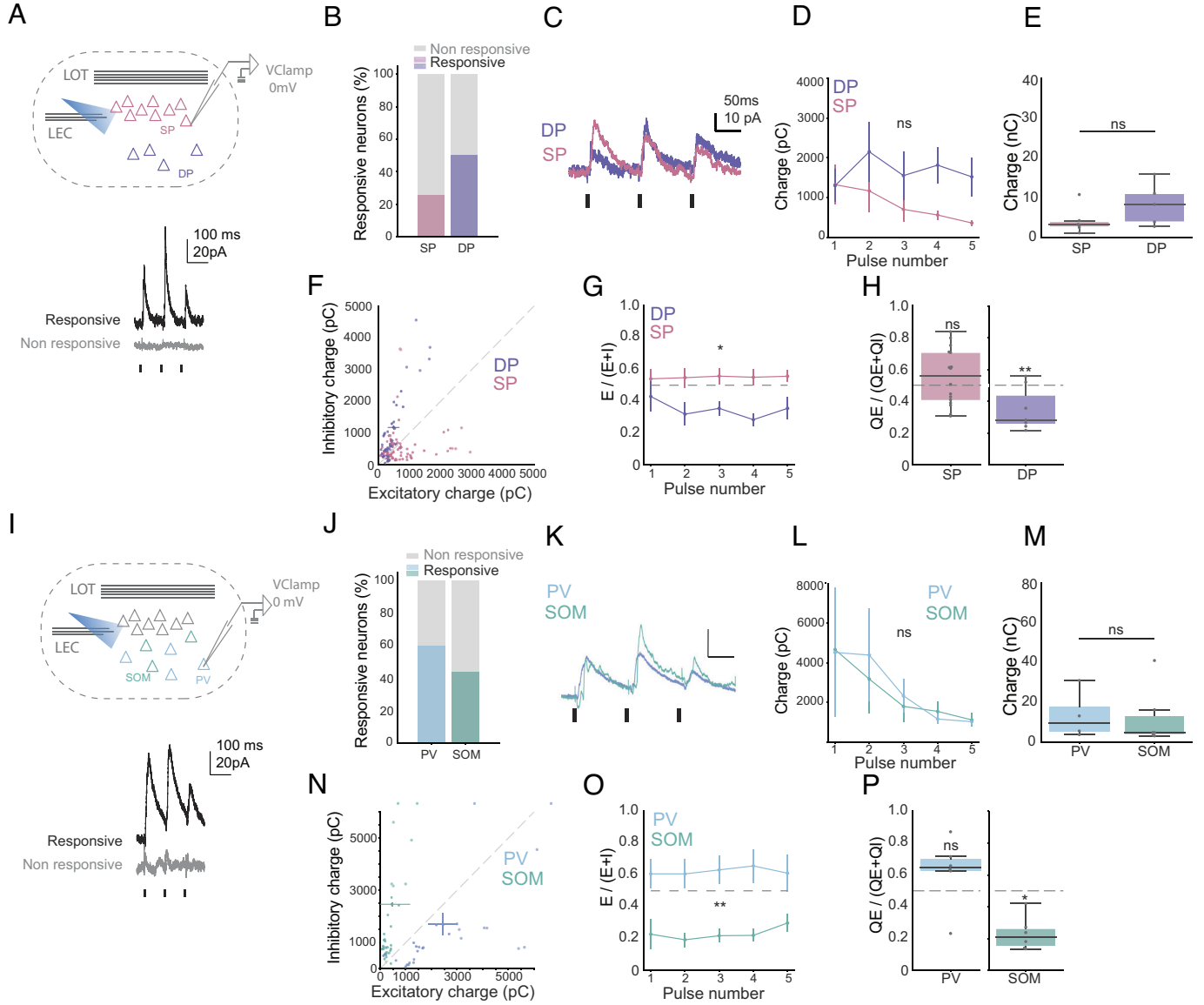

Fig. 3. Activation of LEC input recruits inhibitory circuits in PCx. (*A–E*) Whole-cell recordings of IPSCs evoked by LEC stimulation in pyramidal neurons. (*A*) *Top*: Scheme illustrating experimental procedure. Individual SP and DP neurons are recorded in voltage-clamp holding the membrane at Vh = 0 mV while stimulating with blue light delivered at 10 Hz in a 5-pulses train. *Bottom*: Representative traces of a responsive neuron (black) and a nonresponsive neuron (gray). Black rectangles represent each stimulation pulse (only the first 3 pulses are shown). (Scale bar, x = 100 ms, y = 20 pA.) (*B*) Percentage of SP and DP responsive neurons (25% of SP, nSP = 20 cells from 7 mice; 50% of DP neurons, nDP = 10 cells from 6 mice). (*C*) Representative traces of a SP and a DP IPSC. (Scale bar, x = 50 ms, y = 10 pA.) (*D*) Charge of IPSC evoked by each pulse of LEC stimulation train in SP and DP responsive neurons (two-way ANOVA, SP versus DP: F = 1.78, *P* = 0.2181; variation in pulse number: F = 1.938, *P* = 0.1713; interaction: F = 1.871, *P* = 0.1397; n_{SP} = 5 cells from 4 mice, n_{DP} = 5 cells from 5 mice). (*E*) Total charge of IPSCs evoked by the stimulation train (*t* test, SP versus DP: *t* = 1.337, *P* = 0.2181; n_{SP} = 5 cells, n_{DP} = 5 cells). (*F–H*) Excitation to inhibition balance for pyramidal neurons. (*F*) Pairs of excitatory and inhibitory charge (all pulses are pooled). Highlighted dots illustrate mean and SEM for each neuronal population (nSP = 16 cells from 5 mice, nDP = 7 cells from 4 mice). (*G*) E/I balance calculated as excitatory charge over the sum of excitatory and inhibitory charge evoked by LEC for each pulse of the train (two-way ANOVA, SP versus DP: F = 7.27, *P* = 0.0135; variation in pulse number: F = 1.053, *P* = 0.3748; interaction: F = 1.309, *P* = 0.2735; n_{SP} = 16 cells from 5 mice, n_{DP} = 7 cells from 4 mice). (*H*) Mean E/I balance for SP and DP neurons (*t* test, SP versus 0.5: *t* = 1.642, *P* = 0.1215, n = 16 cells from 5 mice; DP versus 0.5: *t* = 4.956, *P* = 0.0043, n = 7 cells from 4 mice). (*I–M*) Whole-cell recordings of IPSCs evoked by LEC stimulation in inhibitory interneurons. (*I*) *Top*: Scheme illustrating experimental procedure. Individual PV and SOM interneurons are recorded in voltage-clamp holding the membrane at Vh = 0 mV while stimulating with blue light delivered at 10 Hz in a 5-pulses train. *Bottom*: Representative traces of a responsive neuron (black) and a nonresponsive neuron (gray). Black rectangles represent each stimulation pulse (only the first 3 pulses are shown). (Scale bar, x = 100 ms, y = 20 pA.) (*J*) Percentage of PV and SOM responsive neurons (n_{SP} = 20 cells from 7 mice; n_{DP} = 10 cells from 6 mice). (*K*) Representative traces of a PV and a SOM IPSC. (Scale bar, x = 50 ms, y = 100 pA.) (*L*) Charge of IPSC evoked by each pulse of LEC stimulation train in PV and SOM responsive neurons (two-way ANOVA, PV versus SOM: F = 0.0153, *P* = 0.9044; variation in pulse number: F = 2.641, *P* = 0.1385; interaction: F = 0.1159, *P* = 0.976; n_{PV} = 4 cells from 2 mice, n_{SOM} = 6 cells from 5 mice). (*M*) Total charge of IPSCs evoked by the stimulation train (Mann–Whitney test, *P* = 0.6095). (*N–P*) Excitation to inhibition balance for inhibitory neurons. (*N*) Pairs of excitatory and inhibitory charge (all pulses are pooled). Highlighted dots illustrate mean and SEM for each neuronal population. (*O*) E/I balance calculated as excitatory charge over the sum of excitatory and inhibitory charge evoked by LEC for each pulse of the train (two-way ANOVA, PV versus SOM: F = 16.33, *P* = 0.0024; variation in pulse number: F = 0.458, *P* = 0.5953; interaction: F = 0.6095, *P* = 0.6581; n_{PV} = 6 cells from 2 mice, n_{SOM} = 6 cells from 5 mice). (*P*) Mean E/I balance for PV and SOM neurons (Wilcoxon signed-rank test, PV vs. 0.5: W = 11, *P* = 0.3125, n = 6 cells; SOM versus 0.5: W = −21, *P* = 0.0313, n = 6 cells).

decreased for ITI = 25 ms (*SI Appendix*, Fig. S2 *B* and *C*). This suggests that LEC-induced inhibition occurs around 25 ms after the activation and could contract the summation window of DP neurons, perhaps generating a coincidence detector mechanism of LOT and LEC inputs. In agreement with that, we noticed that the distribution of spikes elicited by the first pulse became sharper when LOT and LEC were stimulated (SD_{LOT} = 3.6 ms, $SD_{LOT+LEC}$ = 2.17 ms) (*SI Appendix*, Fig. S2*D*).

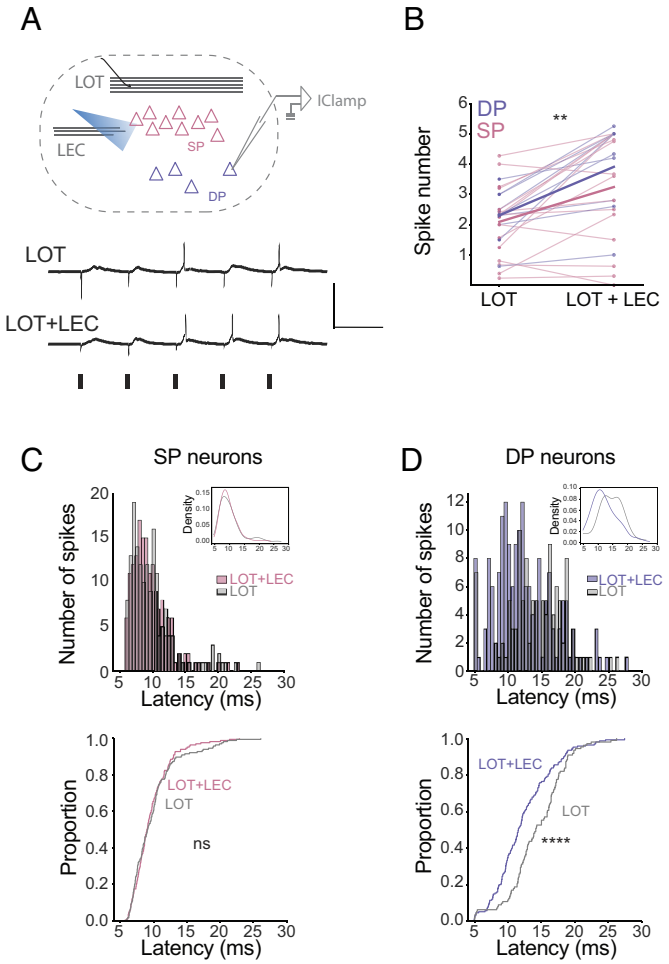

Fig. 4. LEC activation modulates pyramidal spiking responses to OB afferent input. (*A*) *Top*: Scheme illustrating experimental procedure. Individual SP and DP neurons are recorded in current-clamp mode. LOT is stimulated electrically with a 5-pulses train delivered at 10 Hz frequency and threshold intensity. LEC is stimulated with blue light in a 5-pulses train at 10 Hz. *Bottom*: Representative traces showing spiking in response to either LOT stimulation or simultaneous LOT and LEC stimulation. (Scale bar, x = 100 ms, y = 1 V.) (*B*) Total number of action potentials in response to LOT train stimulation or combined LOT and LEC simultaneous stimulation (paired *t* test, SP_{LOT} versus $SP_{LOT+LEC}$: $t = 3.374$, $P = 0.0042$, n = 16 pairs from 10 mice; DP_{LOT} versus $DP_{LOT+LEC}$: $t = 4.371$, $P = 0.0024$, n = 9 pairs from 7 mice). (*C*) *Top*: Histogram showing the distribution of latencies to spike occurrence for SP neurons (all pulses are pooled). *Inset*: Kernel density estimation for LOT (gray) and LOT+LEC (pink) distributions. *Bottom*: Cumulative distribution of latencies in response to LOT stimulation (gray) or combined LOT and LEC stimulation (pink) (Kolmogorov–Smirnov test, statistic = 0.0667, $P = 0.8584$, $n_{LOT} = 165$ spikes, $n_{LOT+LEC} = 165$ spikes). (*D*) *Top*: Histogram showing the distribution of latencies to spike occurrence for DP neurons (all pulses are pooled). *Inset*: Kernel density estimation for LOT (gray) and LOT+LEC (blue) distributions. *Bottom*: Cumulative distribution of latencies in response to LOT stimulation (gray) or combined LOT and LEC stimulation (blue) (Kolmogorov–Smirnov test, statistic = 0.2803, $P < 0.0001$, $n_{LOT} = 112$ spikes, $n_{LOT+LEC} = 175$ spikes).

Discussion

In this work, we found that LEC inputs are heterogeneously distributed in the PCx microcircuit. Specifically, we observed larger responses in SP neurons and PV interneurons compared to DP neurons and SOM interneurons (Fig. 1). Consistent with this result, our analysis revealed a preferential connection of LEC terminals with SP and PV neurons (Fig. 2*C*). Interestingly, we found that LEC inputs differentially affect the inhibitory circuits of the PCx, activating PV while suppressing SOM interneurons (Fig. 3 and *SI Appendix*, Fig. S1). Furthermore, our experiments demonstrated that LEC activation modulates the responses of pyramidal neurons to inputs from the LOT. While both SP and DP neurons exhibited an overall increase in spiking response (Fig. 4), LEC activation produced a sharpening of DP neuronal activation by abolishing late components of the response to LOT (Fig. 4 and *SI Appendix*, Fig. S2). These findings hint at a mechanism whereby LEC afferents suppress recurrent activity through the activation of PV interneurons (Fig. 5), suggesting a role that could switch responses to favor LOT over ASSN.

LEC Functional Connectivity in the PCx Microcircuit. Our recordings show that different classes of PCx neurons exhibited both EPSCs and IPSCs in response to LEC stimulation. However, neurons that were directly contacted (SP and PV neurons) displayed predominantly excitatory responses (a higher E/I balance) while neurons that responded primarily to the recurrent activity recruited by LEC showed a predominant inhibitory component in their responses (DP and SOM, with a lower E/I balance). Heterogeneous distribution of afferent inputs has also been previously observed in the contacts that the Basolateral amygdala (BLA) establishes with the PCx (38), where DP and PV neurons were preferentially contacted. The difference of both types of inputs arriving from higher processing areas suggests that each input differentially organizes the activity in PCx, with BLA preferentially activating DP neurons and LEC preferentially activating SP neurons. However,

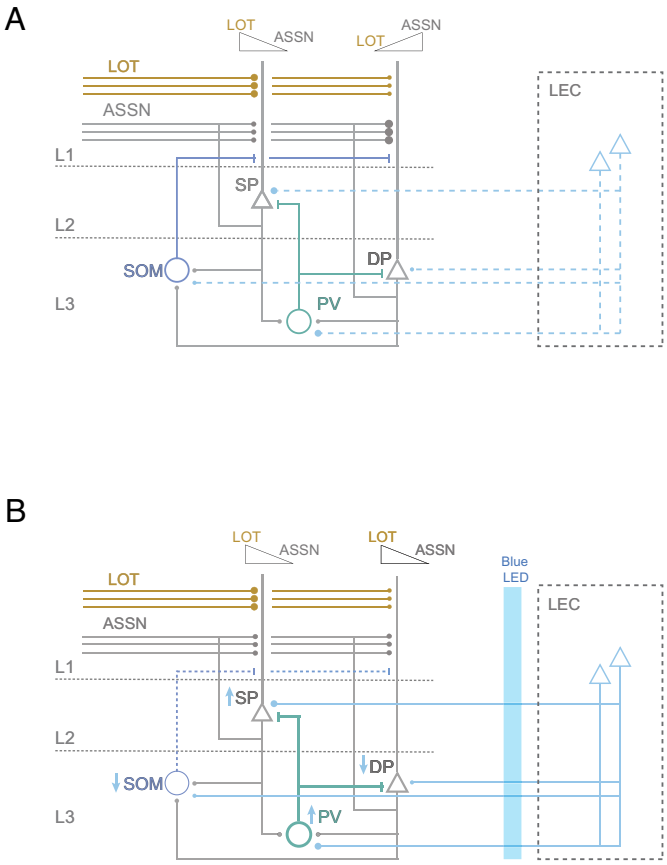

Fig. 5. Reorganization of PCx inputs induced by LEC activation. (*A*) Sensory afferents arriving from the olfactory bulb through the LOT contact pyramidal neurons and also recruit ASSN circuit. SP neurons receive a larger fraction of LOT inputs than DP neurons. Conversely, DP neurons receive more inputs from ASSN compared with SP neurons. PV and SOM interneurons are recruited in a feedback manner by PCx principal neurons. PV interneurons contact pyramidal neurons at the soma, while SOM interneurons target the proximal apical dendrites. (*B*) Optogenetic activation of excitatory LEC projections reconfigures PCx microcircuit. PV interneurons are directly activated by LEC inputs, leading to a decrease in network excitatory recurrence. SOM interneurons are indirectly silenced by LEC activation disinhibiting apical dendrites of pyramidal neurons. This differential effect of LEC on PCx inhibitory circuits provokes an increase in pyramidal neurons' response to LOT input while reducing their response to ASSN.

both inputs produce strong activation of PV neurons, suggesting a common mechanism to inhibit recurrent activity.

In this study, we did not investigate how LEC inputs affect semilunar (SL) cells located in superficial layer 2, which process olfactory information in parallel to pyramidal cells (39). Although these neurons receive robust inputs from the LOT on their distal apical dendrites, they lack basal dendrites and have minimal excitatory intracortical inputs (7, 39, 40). Consequently, LEC afferents may not strongly modulate these cells. However, further research is necessary to test this hypothesis and understand their role in processing LEC inputs.

Inhibitory Circuits Recruited by LEC. Previous studies have demonstrated that lesions in the LEC of rats lead to an increased neuronal activity in the PCx at the population level (25). Based on this, it is argued that the LEC has a suppressive function on the PCx, consistent with an inhibition involving local inhibitory circuits. In this study, we were able to test this hypothesis and, furthermore, demonstrate that the inhibitory circuit involved is mediated by PV interneurons.

Although PV interneurons also receive inhibition, stimulation of LEC terminals was sufficient to trigger action potential firing from these neurons (*SI Appendix*, Fig. S1). The activation of PV interneurons would have a negative effect on the recurrence of the circuit since these target principal neurons and control their spiking activity (19, 20).

On the other hand, the silencing of SOM interneurons would promote a disinhibition at the level of dendrites in layer 1b. This would lead to enhanced integration of sensory afferents explaining the increase in the early spiking response of pyramidal neurons. It might also enable plasticity. It has been recently shown that SOM disinhibition facilitates long-term potentiation of the ASSN pathway after being associated with strong LOT stimulation (19). The inputs that drive this disinhibition in physiological conditions are not known. We hypothesize that LEC afferents could be involved in such a mechanism, but further experiments should be carried out in order to prove this idea.

Overall, the differential impact of LEC on these two populations of inhibitory interneurons implies that its activation promotes a PCx microcircuit that is more sensitive to inputs from the LOT, while simultaneously reducing recurrence, thereby decreasing the response to this pathway.

LEC Effect in Pyramidal Neurons' Response to LOT. The temporal spiking pattern of neurons within PCx circuit plays a crucial role in neural dynamics. In vivo, global inhibition gives rise to narrow temporal windows of opportunity for generating an action potential (12). Neurons with slower activation kinetics are effectively silenced by inhibitory connections (12, 15, 18, 41). In our results of spiking latencies in response to stimulation of the LOT, both SP and DP neuronal populations displayed a dual-peaked distribution, with peaks around 10 ms and 20 ms, consistent with prior findings (13, 14). We interpreted this bimodal distribution as arising from an early response to the afferent LOT pathway and a delayed response to recurrent activation of the ASSN pathway. This interpretation is supported by the observation that SP neurons, which exhibit strong responses to the afferent pathway, predominantly manifest an early response, while DP neurons, more sensitive to the ASSN pathway, display a pronounced delayed response.

Upon simultaneous stimulation of LOT and the LEC, we observed a temporal shift in the spiking distribution toward earlier responses. This shift was subtle for SP neurons, as they initially exhibited few late APs. However, for DP neurons, there was a notable decrease in late responses coupled with an increase in early spikes.

As previous studies have shown, single afferent stimulation is typically insufficient to elicit a spiking response in DP neurons (20), indicating that input summation must be necessary to activate them. Changes in inhibition can have profound influence in determining the summation time window of neurons. In hippocampal pyramidal cells, weak inhibition at the dendritic level results in a broad integration window, while a strong perisomatic inhibition enforces precise coincidence detection in the soma (42). Our results in DP neurons show that LEC stimulation narrows down the summation window, which results in the locking of the response to the first afferent pulse, and the suppression of delayed APs.

Previous works have established that spatial information significantly influences PCx spiking activity (2, 3, 43, 44). On the other hand, LEC plays a crucial role in processing object location (30, 33, 45–50), in recognizing associations between objects and contexts in episodes (50), in associating attributes that define an environment (51), and in forming cognitive maps of nonspatial elements during olfactory learning (52). This evidence, together with our results showing that LEC projections establish monosynaptic connections with PCx neurons and modulate the network activity, identify the LEC as a strong candidate to provide information about other nonolfactory aspects of the sensory experience to the representation of odors in the PCx.

The findings of this study demonstrate that LEC afferents exert distinct effects on the neuronal populations that compose the piriform cortex circuit. Activation of local inhibitory circuits mediated by PV interneurons leads to a dampening of recurrent activity. Conversely, inhibition of SOM interneurons results in dendritic disinhibition, facilitating enhanced integration of afferent signals. In essence, LEC activation induces a reorganization of inputs within the circuit, favoring dominance of the LOT pathway over the ASSN pathway. This could be interpreted as an attention mechanism toward a specific olfactory stimulus modulated by contextual signals, perhaps increasing odor discrimination.

Future experiments would be important to gain a deeper comprehensive understanding of the interaction between the LEC and PCx. These should include investigating how the LEC modulates other classes of neurons within the PCx (18). Additionally, exploring the specific group of LEC neurons that project to the PCx and modulate its activity, as well as the extent to which PCx afferents that project back to the LEC contribute to the interactions between these regions in vivo, would be highly valuable (28, 53). These insights are crucial to ultimately understand how sensory experience is transformed into a richer representation of odor objects in the brain.

Data, Materials, and Software Availability. Data for the manuscript figures are available at Figshare (https://doi.org/10.6084/m9.figshare.27316101.v1) (54).

ACKNOWLEDGMENTS. We thank members of the Marin-Burgin lab, the Refojo lab, and Muraro lab for insightful discussions. We acknowledge International Development Research Centre IDRC108878 (A.M.-B.), Argentine Agency for the Promotion of Science and Technology, PICT2020-00360 (A.M.-B.), PICT 2020-1536 (N.F.), Swiss National Science Foundation SPIRIT 216044 (A.M.-B.), and FOCEM-Mercosur COF 03/11.

Author affiliations: [a]Instituto de Investigación en Biomedicina de Buenos Aires-Consejo Nacional de Investigaciones Científicas y Técnicas-Partner Institute of the Max Planck Society, Buenos Aires C1425FQD, Argentina

1. J. Poort *et al.*, Learning enhances sensory and multiple non-sensory representations in primary visual cortex. *Neuron* **86**, 1478–1490 (2015).
2. C. Poo, G. Agarwal, N. Bonacchi, Z. F. Mainen, Spatial maps in piriform cortex during olfactory navigation. *Nature* **601**, 595–599 (2022).
3. N. Federman, S. A. Romano, M. Amigo-Duran, L. Salomon, A. Marin-Burgin, Acquisition of non–olfactory encoding improves odour discrimination in olfactory cortex. *Nat. Commun.* **15**, 5572 (2024).
4. M. S. Kehl *et al.*, Single-neuron representations of odours in the human brain. *Nature* **634**, 626–634 (2024), 10.1038/s41586-024-08016-5.
5. J. A. Gottfried, Central mechanisms of odour object perception. *Nat. Rev. Neurosci.* **11**, 628–641 (2010).
6. D. A. Wilson, R. M. Sullivan, Cortical processing of odor objects. *Neuron* **72**, 506–519 (2011).
7. J. M. Bekkers, N. Suzuki, Neurons and circuits for odor processing in the piriform cortex. *Trends Neurosci.* **36**, 429–438 (2013).
8. K. M. Igarashi *et al.*, Parallel mitral and tufted cell pathways route distinct odor information to different targets in the olfactory cortex. *J. Neurosci.* **32**, 7970–7985 (2012).
9. K. M. Franks *et al.*, Recurrent circuitry dynamically shapes the activation of piriform cortex. *Neuron* **72**, 49–56 (2011).
10. A. Hagiwara, S. Pal, T. Sato, M. Wienisch, V. Murthy, Optophysiological analysis of associational circuits in the olfactory cortex. *Front. Neural Circuits* **6**, 18 (2012).
11. D. M. Johnson, K. R. Illig, M. Behan, L. B. Haberly, New features of connectivity in piriform cortex visualized by intracellular injection of pyramidal cells suggest that "primary" olfactory cortex functions like "association" cortex in other sensory systems. *J. Neurosci.* **20**, 6974–6982 (2000).
12. C. Poo, J. S. Isaacson, Odor representations in olfactory cortex: "Sparse" coding, global inhibition, and oscillations. *Neuron* **62**, 850–861 (2009).
13. C. Poo, J. S. Isaacson, A major role for intracortical circuits in the strength and tuning of odor-evoked excitation in olfactory cortex. *Neuron* **72**, 41–48 (2011).
14. H. F. Wiegand *et al.*, Complementary sensory and associative microcircuitry in primary olfactory cortex. *J. Neurosci.* **31**, 12149–12158 (2011).
15. C. C. A. Stokes, J. S. Isaacson, From dendrite to soma: Dynamic routing of inhibition by complementary interneuron microcircuits in olfactory cortex. *Neuron* **67**, 452–465 (2010).
16. N. Suzuki, M. L. S. Tantirigama, K. P. Aung, H. H. Y. Huang, J. M. Bekkers, Fast and slow feedforward inhibitory circuits for cortical odor processing. *eLife* **11**, e73406 (2022).
17. N. Suzuki, J. M. Bekkers, Inhibitory interneurons in the piriform cortex. *Clin. Exp. Pharmacol. Physiol.* **34**, 1064–1069 (2007).
18. N. Suzuki, J. M. Bekkers, Distinctive classes of GABAergic interneurons provide layer-specific phasic inhibition in the anterior piriform cortex. *Cereb. Cortex* **20**, 2971–2984 (2010).
19. M. Canto-Bustos, F. K. Friason, C. Bassi, A.-M.M. Oswald, Disinhibitory circuitry gates associative synaptic plasticity in olfactory cortex. *J. Neurosci.* **42**, 2942–2950 (2022).
20. A. M. Large, N. A. Kunz, S. L. Mielo, A.-M.M. Oswald, Inhibition by somatostatin interneurons in olfactory cortex. *Front. Neural Circuits* **10**, 62 (2016).
21. J. F. Sturgill, J. S. Isaacson, Somatostatin cells regulate sensory response fidelity via subtractive inhibition in olfactory cortex. *Nat. Neurosci.* **18**, 531–535 (2015).
22. K. A. Bolding, K. M. Franks, Recurrent cortical circuits implement concentration-invariant odor coding. *Science* **361**, eaat6904 (2018).
23. K. R. Illig, Projections from orbitofrontal cortex to anterior piriform cortex in the rat suggest a role in olfactory information processing. *J. Comp. Neurol.* **488**, 224–231 (2005).
24. K. Majak, S. Rönkkö, S. Kemppainen, A. Pitkänen, Projections from the amygdaloid complex to the piriform cortex: A PHA-L study in the rat. *J. Comp. Neurol.* **476**, 414–428 (2004).
25. J. Chapuis *et al.*, Lateral entorhinal modulation of piriform cortical activity and fine odor discrimination. *J. Neurosci.* **33**, 13449–13459 (2013).
26. K. L. Agster, R. D. Burwell, Cortical efferents of the perirhinal, postrhinal, and entorhinal cortices of the rat. *Hippocampus* **19**, 1159–1186 (2009).
27. A. Diodato *et al.*, Molecular signatures of neural connectivity in the olfactory cortex. *Nat. Commun.* **7**, 12238 (2016).
28. Y. J. Zhang, J. Y. Lee, K. M. Igarashi, Circuit dynamics of the olfactory pathway during olfactory learning. *Front. Neural Circuits* **18**, 1437575 (2024).
29. F. C. Leitner *et al.*, Spatially segregated feedforward and feedback neurons support differential odor processing in the lateral entorhinal cortex. *Nat. Neurosci.* **19**, 935–944 (2016).
30. S. S. Deshmukh, J. J. Knierim, Representation of non-spatial and spatial information in the lateral entorhinal cortex. *Front. Behav. Neurosci.* **5**, 69 (2011).
31. K. M. Igarashi, L. Lu, L. L. Colgin, M.-B. Moser, E. I. Moser, Coordination of entorhinal-hippocampal ensemble activity during associative learning. *Nature* **510**, 143–147 (2014).
32. H. Jun *et al.*, Prefrontal and lateral entorhinal neurons co-dependently learn item–outcome rules. *Nature* **633**, 864–871 (2024), 10.1038/s41586-024-07868-1.
33. A. Tsao, M.-B. Moser, E. I. Moser, Traces of experience in the lateral entorhinal cortex. *Curr. Biol.* **23**, 399–405 (2013).
34. B. J. Young, T. Otto, G. D. Fox, H. Eichenbaum, Memory representation within the parahippocampal region. *J. Neurosci.* **17**, 5183–5195 (1997).
35. O. M. Bilash, S. Chavlis, C. D. Johnson, P. Poirazi, J. Basu, Lateral entorhinal cortex inputs modulate hippocampal dendritic excitability by recruiting a local disinhibitory microcircuit. *Cell Rep.* **42**, 111962 (2023).
36. P. Salvan *et al.*, Frequency modulation of entorhinal cortex neuronal activity drives distinct frequency-dependent states of brain-wide dynamics. *Cell Rep.* **37**, 109954 (2021).
37. W. Xu, D. A. Wilson, Odor-evoked activity in the mouse lateral entorhinal cortex. *Neuroscience* **223**, 12–20 (2012).
38. V. M. Luna, A. Morozov, Input-specific excitation of olfactory cortex microcircuits. *Front. Neural Circuits* **6**, 69 (2012).
39. S. Nagappan, K. M. Franks, Parallel processing by distinct classes of principal neurons in the olfactory cortex. *eLife* **10**, e73668 (2021).
40. J. M. C. Choy *et al.*, Optogenetic mapping of intracortical circuits originating from semilunar cells in the piriform cortex. *Cereb. Cortex* **27**, 589–601 (2017).
41. V. M. Luna, N. E. Schoppa, GABAergic circuits control input-spike coupling in the piriform cortex. *J. Neurosci.* **28**, 8851–8859 (2008).
42. F. Pouille, M. Scanziani, Enforcement of temporal fidelity in pyramidal cells by somatic feed-forward inhibition. *Science* **293**, 1159–1163 (2001).
43. O. McKissick, N. Klimpert, J. T. Ritt, A. Fleischmann, Odors in space. *Front. Neural Circuits* **18**, 1414452 (2024).
44. W. Mena *et al.*, Differential encoding of odor and place in mouse piriform and entorhinal cortex. bioRxiv [Preprint] (2023). https://doi.org/10.1101/2023.10.05.561119 (Accessed 8 October 2023).
45. Z. Beer, C. Chwiesko, T. Kitsukawa, M. M. Sauvage, Spatial and stimulus-type tuning in the LEC, MEC, POR, PrC, CA1, and CA3 during spontaneous item recognition memory. *Hippocampus* **23**, 1425–1438 (2013).
46. O. Y. Chao, J. P. Huston, J.-S. Li, A.-L. Wang, M. A. de Souza Silva, The medial prefrontal cortex–lateral entorhinal cortex circuit is essential for episodic-like memory and associative object-recognition. *Hippocampus* **26**, 633–645 (2016).
47. M. R. Hunsaker, V. Chen, G. T. Tran, R. P. Kesner, The medial and lateral entorhinal cortex both contribute to contextual and item recognition memory: A test of the binding of items and context model. *Hippocampus* **23**, 380–391 (2013).
48. C. S. Keene *et al.*, Complementary Functional organization of neuronal activity patterns in the perirhinal, lateral entorhinal, and medial entorhinal cortices. *J. Neurosci.* **36**, 3660–3675 (2016).
49. T. Van Cauter *et al.*, Distinct roles of medial and lateral entorhinal cortex in spatial cognition. *Cereb. Cortex* **23**, 451–459 (2013).
50. D. I. G. Wilson *et al.*, Lateral entorhinal cortex is critical for novel object-context recognition. *Hippocampus* **23**, 352–366 (2013).
51. M. V. Kuruvilla, J. A. Ainge, Lateral entorhinal cortex lesions impair local spatial frameworks. *Front. Syst. Neurosci.* **11**, 30 (2017).
52. K. M. Igarashi, J. Y. Lee, H. Jun, Reconciling neuronal representations of schema, abstract task structure, and categorization under cognitive maps in the entorhinal-hippocampal-frontal circuits. *Curr. Opin. Neurobiol.* **77**, 102641 (2022).
53. Y. Chen *et al.*, High-throughput sequencing of single neuron projections reveals spatial organization in the olfactory cortex. *Cell* **185**, 4117–4134.e28 (2022).
54. O. Pedroncini, N. Federman, A. Marin-Burgin, Pedroncini et al data figures. Figshare. https://doi.org/10.6084/m9.figshare.27316101.v1. Deposited 29 October 2024.